2019

Heteroatom-doped MoSe2 Nanosheets with Enhanced Hydrogen Evolution Kinetics for Alkaline Water Splitting

Guoqiang Zhao
University of Wollongong, gz815@uowmail.edu.au

Xingyong Wang
University of Wollongong, xingyong@uow.edu.au

Shaolan Wang
University of Wollongong

Kun Rui
University of Wollongong, krui@uow.edu.au

Yaping Chen
University of Wollongong, yc463@uowmail.edu.au

See next page for additional authors

Heteroatom-doped MoSe2 Nanosheets with Enhanced Hydrogen Evolution Kinetics for Alkaline Water Splitting

Abstract

Electrochemical water splitting for hydrogen generation is a vital part for the prospect of future energy systems, however, the practical utilization relies on the development of highly active and earth-abundant catalysts to boost the energy conversion efficiency as well as reduce the cost. Molybdenum diselenide (MoSe2) is a promising nonprecious metal-based electrocatalyst for hydrogen evolution reaction (HER) in acidic media, but it exhibits inferior alkaline HER kinetics in great part due to the sluggish water adsorption/dissociation process. Herein, the alkaline HER kinetics of MoSe2 is substantially accelerated by heteroatom doping with transition metal ions. Specifically, the Ni-doped MoSe2 nanosheets exhibit the most impressive catalytic activity in terms of lower overpotential and larger exchange current density. The density functional theory (DFT) calculation results reveal that Ni/Co doping plays a key role in facilitating water adsorption as well as optimizing hydrogen adsorption. The present work paves a new way to the development of low-cost and efficient electrocatalysts towards alkaline HER.

Disciplines

Engineering | Physical Sciences and Mathematics

Publication Details

Zhao, G., Wang, X., Wang, S., Rui, K., Chen, Y., Yu, H., Ma, J., Dou, S. Xue. & Sun, W. (2019). Heteroatom-doped MoSe2 Nanosheets with Enhanced Hydrogen Evolution Kinetics for Alkaline Water Splitting. Chemistry: An Asian Journal, 14 (2), 301-306.

Authors

Guoqiang Zhao, Xingyong Wang, Shaolan Wang, Kun Rui, Yaping Chen, Haibo Yu, Jing Ma, Shi Xue Dou, and Wenping Sun

Iron-doped nickel molybdate with enhanced oxygen evolution kinetics

Jiayi Chen,[a] Guoqiang Zhao,[a] Yaping Chen,[a] Kun Rui,[a] Hui Mao,[b,*] Shi Xue Dou,[a] and Wenping Sun[a,*]

Abstract: Electrochemical water splitting is one of potential approaches for making renewable energy production and storage viable. Oxygen evolution reaction (OER), as a sluggish four-electron electrochemical reaction, has to overcome high overpotential to accomplish overall water splitting. Therefore, developing low-cost and highly active OER catalysts is the key for achieving efficient and economical water electrolysis. In this work, Fe-doped $NiMoO_4$ was synthesized and evaluated as the OER catalyst in alkaline medium. Fe^{3+} doping helps to regulate the electronic structure of Ni centers in $NiMoO_4$, which consequently promotes the catalytic activity of $NiMoO_4$. The overpotential to reach a current density of 10 mA cm^{-2} is 299 mV in 1 M KOH for the optimal $Ni_{0.9}Fe_{0.1}MoO_4$, which is 65 mV lower than $NiMoO_4$. Further, the catalyst also shows exceptional performance stability during a 2-h chronopotentiometry testing. Moreover, the real catalytically active center of $Ni_{0.9}Fe_{0.1}MoO_4$ is also unraveled based on the *ex-situ* characteristics. These results provide new alternatives for precious metal-free catalysts towards alkaline OER and also expand Fe-doping-induced synergistic effect towards performance enhancement to new catalyst systems.

Introduction

Electrochemical water splitting is one of the most promising energy conversion and storage strategies towards efficient utilization of renewable energy and has drawn ever-increasing research attention recently. During water splitting process, oxygen evolution reaction (OER) at the anode involves a four-electron-transfer process, which is the main sluggish step for water splitting.[1] To date, noble metal-based materials, such as IrO_2 and RuO_2, are still the leading OER catalysts.[2] Considering the scarcity of noble metals, it is of critical necessity to minimize cost of catalysts for economical water splitting. Therefore, a series of earth-abundant materials, particularly Ni, Co-based materials, have been extensively explored as OER catalysts, and some of them have shown impressive catalytic activities comparable to noble metals.[3] For example, Lu et al. reported three-dimension NiFe layered double hydroxide (LDH) film as electrocatalyst for the OER,[4] and the NiFe LDH film exhibited excellent OER catalytical activity with an overpotential of ~230 mV at 10 mA cm^{-2}, which is lower than the commercial 20 wt% IrO_2/C catalyst. On the other hand, structural engineering is an effective approach in view of exposing more active sites as well as realizing rapid mass diffusion, which is vital for constructing highly active and stable electrocatalysts.[5] Recently, nanosheet-like nanostructures are emerging fast into electrocatalysis field owing to the unique physicochemical properties, including abundant edge sites, highly exposed active centers, and easily tuned electronic structures.[6] Various kinds of nanosheets-based nanostructures have shown interesting electrocatalytic activity towards water splitting.[7]

In this work, nickel molybdate ($NiMoO_4$) with a flower-like nanostructure composed of nanosheets was synthesized via a hydrothermal process followed by annealing in air and were evaluated as OER catalysts in 1 M KOH. The dependence of Fe doping on the catalytic activity of $NiMoO_4$ was studied, and the results demonstrate that Fe doping can significantly promote the OER kinetics. Detailed electrochemical tests prove that the Fe-doping-induced synergistic effect should be responsible for the performance improvement. Besides, the real active centers in Fe-doped $NiMoO_4$ were also investigated.

Results and Discussion

The Fe-doped $NiMoO_4$ ($Ni_{1-x}Fe_xMoO_4$, x=0, 0.05, 0.1 and 0.2) were synthesized via a hydrothermal process followed by annealing at 500 °C in air. The crystal phase of $Ni_{1-x}Fe_xMoO_4$ was confirmed by X-ray diffraction (XRD) patterns (**Figure 1**a), and the results reveal the formation of β-$NiMoO_4$ (JCPDS No. 45-0142).[8] No characteristic diffraction peaks of iron oxide-based phases are observed, implying the successful doping of Fe atoms into $NiMoO_4$ lattice. However, it should be noted that the relative density of (220) peak at 26.6° decrease with increasing Fe content. It can be explained that, Fe-O bond distance is shorter than Ni-O bond distance, and thus the $NiMoO_4$ lattice structure is changed when Ni atoms are partially replaced by Fe atoms.[9]

The scanning electron microscope (SEM) image of $Ni_{0.9}Fe_{0.1}MoO_4$ shows a clear flower-like structure composed of nanosheets (Figure S1, Supporting Information). The SEM-EDS mapping (Figure S2, Supporting Information) reveals that Ni, Fe, Mo and O distribute very homogeneously in $Ni_{0.9}Fe_{0.1}MoO_4$. Transmission electron microscope (TEM) image of the $Ni_{0.9}Fe_{0.1}MoO_4$ in Figure 1b reveals a rough and porous surface morphology, which is similar to $NiMoO_4$ (Figure S3, Supporting Information). The BET surface area of $Ni_{0.9}Fe_{0.1}MoO_4$ and $NiMoO_4$ is determined to be 156 and 141 m^2 g^{-1}, respectively (Figure S3, Supporting Information), illustrating that the unique morphology ensures a large surface area and abundant active sites for the OER reaction. Meanwhile, as shown in Figure 1c, the labled lattice spacing of 0.24 and 0.26 nm can be assigned to the (400) and (31-2) crystal planes of $Ni_{0.9}Fe_{0.1}MoO_4$, respectively,[10] corresponding well with the inset fast four transform (FFT) result. Besides, the selected area electron diffraction (SAED) of $Ni_{0.9}Fe_{0.1}MoO_4$ is ascribed to a typical β-

[a] J. Chen, G. Zhao, Y. Chen, Dr. K. Rui, Prof. S. X. Dou, Dr. W. Sun
Institute for Superconducting and Electronic Materials, Australian Institute for Innovative Materials, University of Wollongong, Wollongong, NSW 2522, Australia
E-mail: wenping@uow.edu.au
[b] Dr. H. Mao
College of Chemistry and Materials Science, Sichuan Normal University, Chengdu 610068, P. R. China
E-mail: rejoice222@163.com
Supporting information for this article is given via a link at the end of the document.

$NiMoO_4$ phase (Figure 1d), further demonstrating the successful doping of Fe.[10a]

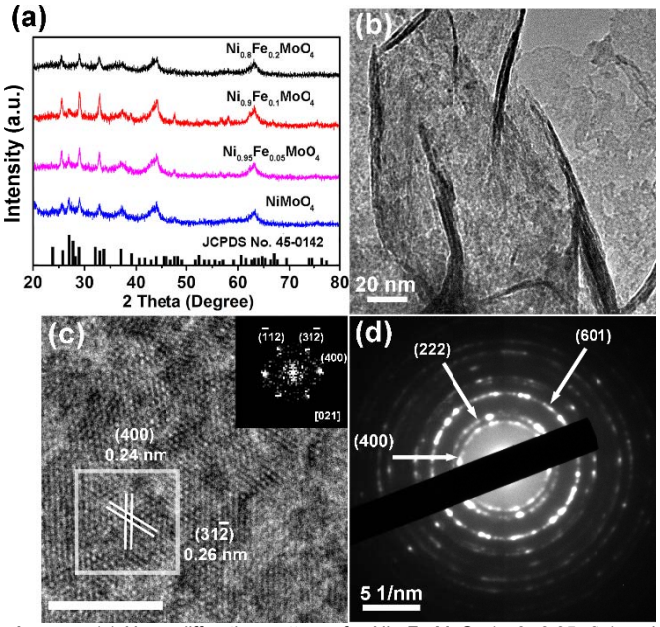

Figure 1. (a) X-ray diffraction patterns for $Ni_{1-x}Fe_xMoO_4$ (x=0, 0.05, 0.1 and 0.20). (b, c) TEM and HRTEM images of $Ni_{0.9}Fe_{0.1}MoO_4$. Inset: FFT pattern of the selected region. (d) SAED pattern of $Ni_{0.9}Fe_{0.1}MoO_4$.

X-ray photoelectron spectroscopy (XPS) was carried out to investigate surface compositions and valence states of the $Ni_{0.9}Fe_{0.1}MoO_4$ and $NiMoO_4$. The coexistence of Ni, Fe, Mo and O species can be clearly demonstrated by the survey spectra (**Figure 2**a). The Ni 2p XPS spectrum of the $NiMoO_4$ show two main peaks at 855.2 eV and 872.9 eV,[11] which can be assigned to typical peaks of Ni^{2+}. (Figure 2b). For $Ni_{0.9}Fe_{0.1}MoO_4$,

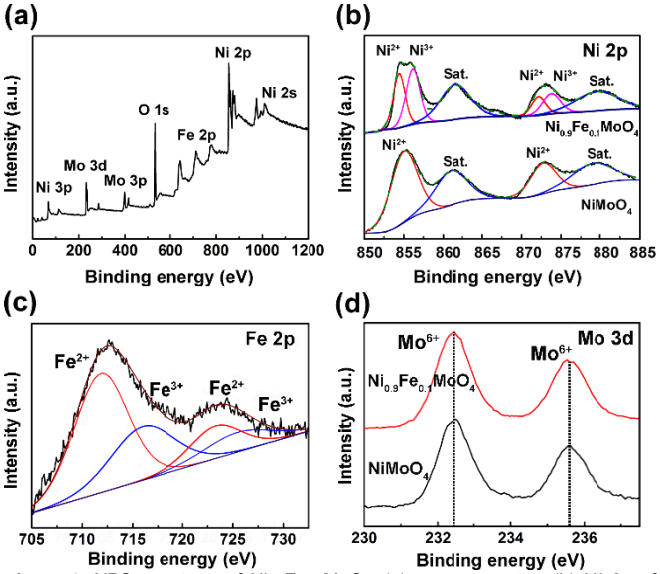

Figure 2. XPS spectrum of $Ni_{0.9}Fe_{0.1}MoO_4$: (a) survey spectra, (b) Ni 2p of $Ni_{0.9}Fe_{0.1}MoO_4$ and $NiMoO_4$, (c) Fe 2p, and (d) Mo 3d of $Ni_{0.9}Fe_{0.1}MoO_4$ and $NiMoO_4$.

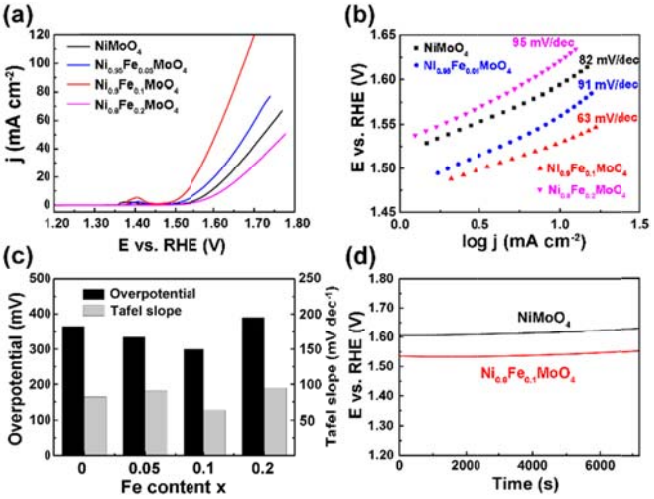

Figure 3. Electrochemical performance. (a) Polarization curves and (b) Tafel curves of $Ni_{1-x}Fe_xMoO_4$ (x=0, 0.05, 0.1 and 0.20) in 1 M KOH (c) Overpotential at 10 mA cm^{-2} and Tafel slope derived from LSV curves, (d) Chronopotentiometry test of $Ni_{0.9}Fe_{0.1}MoO_4$ and $NiMoO_4$ at a constant current density of 10 mA cm^{-2}.

the peak at ~855 eV in the Ni 2p XPS spectrum prove the presence of two chemical environments for nickel atoms (Figure 2b). The spectrum was fitted by considering two resolved doublets at 854.5/872.2 eV and 856.2/873.9 eV, corresponding to Ni^{2+} and Ni^{3+}, respectively.[12] The proportion of Ni^{2+} and Ni^{3+} species is calculated to be 44% and 56%, respectively. Compared with $NiMoO_4$, the appearance of Ni^{3+} can be attributed to the electron transfer from Ni to the doped Fe.[12b, 13] The Fe 2p XPS spectrum of the $Ni_{0.9}Fe_{0.1}MoO_4$ in Figure 2c is deconvoluted into four fitted peaks, indicating the coexistence of Fe^{3+} (711.9 and 724.4 eV) and Fe^{2+} (716.0 and 726.3 eV).[12b, 14] Figure 2d shows Mo 3d XPS spectrums of $Ni_{0.9}Fe_{0.1}MoO_4$ and $NiMoO_4$, in which both of the doublet peaks locate at 235.6 eV and 232.4 eV, corresponding to Mo $3d_{3/2}$ and Mo $3d_{5/2}$ of Mo^{6+} species, respectively. Unlike Ni, the valence state of Mo does not change after Fe doping.

The OER electrocatalytic performance of the $Ni_{1-x}Fe_xMoO_4$ was tested in a typical three electrodes system in 1 M KOH. The LSV curve of the $NiMoO_4$ shows an oxidation peak at 1.37 V (vs. RHE) due to the oxidation of Ni^{2+} to Ni^{3+} (**Figure 3**a). Notably, the oxidation peak shifts positively after Fe incorporation, which is attributed to the valence state change of Ni after Fe doping, and it is also a specific indicator to determine whether Fe is doped into $NiMoO_4$.[9a, 15] $Ni_{0.95}Fe_{0.05}MoO_4$ and $Ni_{0.9}Fe_{0.1}MoO_4$ show higher OER activity than $NiMoO_4$. $Ni_{0.9}Fe_{0.1}MoO_4$ requires an overpotential of 299 mV to generate an anodic current of 10 mA cm^{-2}, which is 65 mV lower than $NiMoO_4$ (364 mV). Tafel plots were constructed from polarization curves to study the OER kinetics of the electrocatalysts (Figure 3b).[16] The Tafel slope of $Ni_{0.9}Fe_{0.1}MoO_4$ is calculated to be 63 mV dec^{-1}, which is lower than $NiMoO_4$ (82 mV dec^{-1}), illustrating an accelerated OER kinetics of $Ni_{0.9}Fe_{0.1}MoO_4$. The overpotentials (10 mA cm^{-2}) and Tafel slopes of $Ni_xFe_{1-x}MoO_4$ are displayed in Figure 3c.

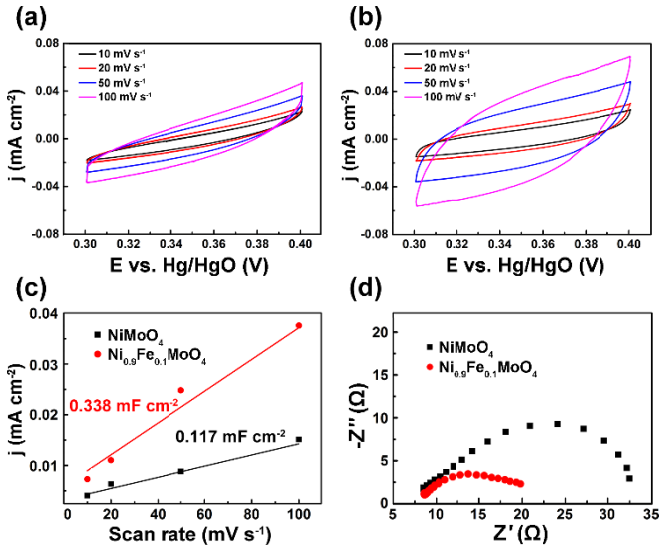

Figure 4. (a, b) CV curves of $Ni_{0.9}Fe_{0.1}MoO_4$ and $NiMoO_4$ performed from 0.3 to 0.4 V (vs. Hg/HgO) at different scan rates (10, 20, 50, 100 mV s^{-1}), respectively. (c) the fitted result of C_{DL} (d) Electrochemical impedance spectra of $Ni_{0.9}Fe_{0.1}MoO_4$ and $NiMoO_4$.

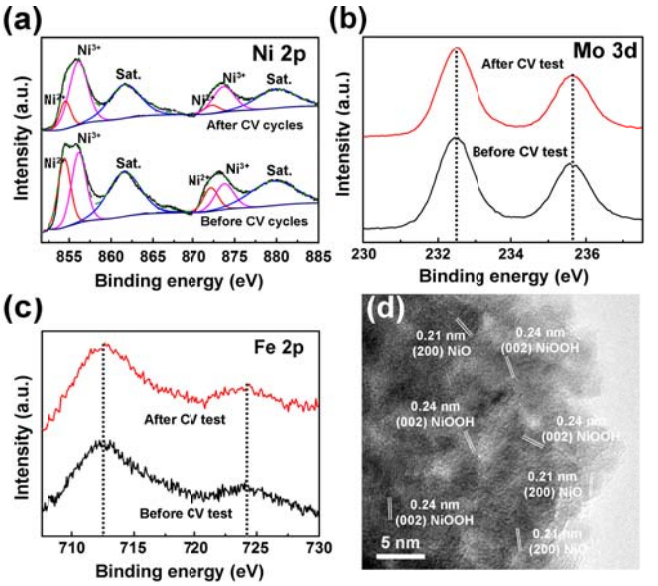

Figure 5. (a-c) High-resolution XPS spectra of the Ni 2p, Mo 3d and Fe 2p for $Ni_{0.9}Fe_{0.1}MoO_4$ before and after CV test, (d) TEM image for $Ni_{0.9}Fe_{0.1}MoO_4$ sample after CV cycles.

The $Ni_{0.9}Fe_{0.1}MoO_4$ exhibit the best OER activity with the minimum overpotential and the smallest Tafel slope, which also exhibit comparable activity to some typical transition metal-based catalysts and commercial IrO_2 (Figure S5, Supporting Information).[17] When the Fe content further increased, $Ni_{0.8}Fe_{0.2}MoO_4$ shows an increased overpotential (390 mV). Besides, the $Ni_{0.9}Fe_{0.1}MoO_4$ electrocatalyst exhibit excellent stability, which was another critical parameter for evaluating electrocatalysts. As indicated by the chronopotentiometry (CP) measurement (Figure 3d), $Ni_{0.9}Fe_{0.1}MoO_4$ shows a slightly increase of potential from 1.54 to 1.55 V (vs. RHE) after running for 2 h at 10 mA cm^{-2}, which reveals a similar stability but a much lower potential as compared with $NiMoO_4$ (increasing from 1.61 to 1.63 V). The excellent stability performance can be related to the porous structure that buffers the volume change through the OER process. Combined with the aforementioned XPS results, the greatly improved OER performance can be attributed to the Fe doping-induced high valence Ni^{3+} in $Ni_{0.9}Fe_{0.1}MoO_4$. The existence of Ni atom in a higher valence state facilitates the surface adsoption of oxygen, and thus endows the Ni-OOH formation, accelerating the OOH species deprotonation to harvest O_2.[13b, 18]

The electrochemically active surface area (ECSA) was explored to study factors of OER activity enhancement. As shown in **Figure 4**a-b, the ECSAs of $Ni_{0.9}Fe_{0.1}MoO_4$ and $NiMoO_4$ were evaluated by the double-layer capacitance (C_{DL}) depend on CV curves measured with non-Faradaic currents. The slope of the fitted plots is C_{DL} (Figure 4c). The C_{DL} of $Ni_{0.9}Fe_{0.1}MoO_4$ is 0.338 mF cm^{-2}, which is three times larger than that of $NiMoO_4$ (0.117 mF cm^{-2}). As illustrated by the BET result of $NiMoO_4$ and $Ni_{0.9}Fe_{0.1}MoO_4$ (Figure S3, Supporting Information), the C_{DL} increment should be mainly derived from the enhanced adsorption capacity promoted by Ni^{3+} after Fe doping.[18a, 19] Furthermore, as shown in the electrochemical impedance spectra (EIS) (Figure 4d), the low-frequency resistance of $Ni_{0.9}Fe_{0.1}MoO_4$ is around 13.1 Ω, which is great smaller than that of $NiMoO_4$ (25.7 Ω), revealing accelerated charge transfer and mass diffusion at the $Ni_{0.9}Fe_{0.1}MoO_4$ electrode/electrolyte interface.[5c, 20]. Both the ECSA and EIS results confirm the excellent electrochemical properties of $Ni_{0.9}Fe_{0.1}MoO_4$ catalyst.

Importantly, *ex-situ* XPS and TEM analysis of the $Ni_{0.9}Fe_{0.1}MoO_4$ after CV cycles were carried out to unravel the real active centers. As shown in **Figure 5**a, we can directly observe Ni $2p_{3/2}$ peak at 856.0 eV shifts positively after CV cycles, suggesting the oxidation state of Ni increases during the catalytic process. The fitted result demonstrate that Ni^{3+} proportion increases from 56% to 79%, which might be due to the formation of NiOOH during the catalytic process.[3f, 13b] Meanwhile, Mo 3d and Fe 2p spectrum keep unchanged (Figure 5b and c). Moreover, as demonstrated by the TEM image in Figure 5d, the lattice spacing of 0.24 nm can be indexed to the (002) crystal plane of hexagonal NiOOH.[21] In addition, interplanar distance of 0.21 nm also can be viewed, which is ascribed to the (111) planes of NiO.[3f, 22] Based on the aforementioned discussion, these results illustrate that Ni is the real active catalytic center of $Ni_{0.9}Fe_{0.1}MoO_4$ catalyst during water oxidation.

Table 1. TOF of $Ni_{0.9}Fe_{0.1}MoO_4$ and $NiMoO_4$

Sample	TOF (s^{-1}) @η=300 mV	TOF (s^{-1}) @η=350 mV
$Ni_{0.9}Fe_{0.1}MoO_4$	0.032	0.106
$NiMoO_4$	0.0042	0.02

The turnover frequency (TOF) was further calculated to evaluate the intrinsic OER catalytic activities of $Ni_{0.9}Fe_{0.1}MoO_4$ and

$NiMoO_4$. As shown in Table 1, the TOF of $Ni_{0.9}Fe_{0.1}MoO_4$ is 0.032 s^{-1} at the overpotential of 300 mV, which is almost six folds higher than that of $NiMoO_4$ (0.0042 s^{-1}). The result further confirms the enhanced intrinsic activity induced by Fe doping. It has to be mentioned that, compared with most Ni-based catalysts such as NiO or $Ni(OH)_2$, the proportion of Ni content is much lower in $Ni_{0.9}Fe_{0.1}MoO_4$, but it deliveres simialr and even better mass activity than NiO [23]. Thus, it can be inferred that, in addition to the oxidation state of Ni, the coordination environment of Ni might also determine the intrinsic activity of Ni active sites.

Conclusions

In summary, $NiMoO_4$-based catalysts were synthesized and evaluated for alkaline OER, and the OER kinetics was substantially enhanced by Fe doping. The optimal $Ni_{0.9}Fe_{0.1}MoO_4$ exhibited a lower overpotential of 299 mV than $NiMoO_4$ (364 mV) at a current density of 10 mA cm^{-2}. Ni species are demonstrated to be the real active sites, and NiOOH/NiO were formed *in situ* during OER. This work demonstrates Fe doping is also an effective strategy for improving the catalytic activity of $NiMoO_4$-based catalysts besides NiO and $Ni(OH)_2$.

Experimental Section

All the chemicals were purchased from Sigma-Aldrich (A.R grade) and used as received without further purification.

Synthesis of $NiMoO_4$ and $Ni_{1-x}Fe_xMoO_4$

$NiMoO_4$ were synthesized via a typical hydrothermal treatment followed by annealing process. 1 mmol of $Ni(NO_3)_2{\cdot}6H_2O$ and 1 mmol of $Na_2MoO_4{\cdot}2H_2O$ were dissolved in 30 mL deionized (DI) water with vigorous stirring. Next, 0.24 g urea was added into the solution. After stirring for 30 min, the final solution was transferred to a 45 mL Teflon lined stainless steel autoclave and kept at 160 °C for 8 h. Fe-doped $NiMoO_4$ was prepared via the similar procedure by altering the molar ratio of $Ni(NO_3)_2{\cdot}6H_2O$ to $Fe(NO_3)_3{\cdot}9H_2O$. For $Ni_{0.9}Fe_{0.1}MoO_4$, 0.1 mmol $Fe(NO_3)_3{\cdot}9H_2O$ and 0.9 mmol $Ni(NO_3)_2{\cdot}6H_2O$ were added in the precursor solution. After the autoclaves were cooled down, the precursor samples were washed with DI water and ethanol three times and dried at 65 °C for 10 h. Finally, the products were kept at 500 °C in air for 2 h to obtain $NiMoO_4$ and $Ni_{1-x}Fe_xMoO_4$.

Characterization of materials

The X-ray diffraction (XRD) was performed using Mac Science XRD (λ = 1.5406 Å, 25 mA, 40 kV, 1° min^{-1} from 20 to 80°). XPS measurements were carried out on a Phoibos 100 analyzer, using monochrome Al Kα (hv=1486.6 eV) as the X-ray excitation source. The sample morphologies were recorded by the field emission scanning electron microscope (SEM, JEOL JSM-7500FA, 10 kV) and transmission electron microscopy (TEM, JEOL JEM-2010, 200 kV). The specific surface areas of the samples were measured by a TriStar II 3020-BET/BJH analyzer.

Electrochemical Measurements

The electrochemical performance were tested by rotating disk electrode system (Pine Instruments, WaveDriver), which were performed in 1 M KOH aqueous solution. The reference and counter electrode is Mercury/Mercuric oxide (Hg/HgO, 1 M KOH) and platinum foil, respectively. The working electrode was a glassy carbon electrode (0.196 cm^{-2}) coated with different catalyst samples. For sample preparation on rotating disk, 2.0 mg catalyst was dispersed in a mixed solution (Nafion solution: 8 μL, deionized water: 192 μL, isopropanol: 100 μL). The mixture was ultrasonicated for 1 h to obtain homogeneous dispersion. 10 μL of the dispersion was coated on the polished GC electrode. The electrode was then dried and used for electrochemical studies. The rotating speed was set at 1600 rpm to prevent O_2 concentrate on the electrode surface. Before LSV test, the catalysts were first activated by CV test (1.0 to 1.7 V vs. RHE, 10 mV s^{-1}) for 30 cycles. LSV polarization curves were acquired at 5 mV s^{-1} to illustrate the catalytic activity, corrected with 95% iR compensation. Chronopotentiometry measurement was performed at 10 mA cm^{-2} to measure the stability performance. EIS was tested at 0.6 V (vs. Hg/HgO) with the frequency ranging from 0.1 to 100 kHz. The ECSA was evaluated by calculated the C_{DL} of the samples based on the CV curves via Equ. (1).[17b] The potential window of CV was 0.3-0.4 V vs. Hg/HgO, and the scan rates were set at 10, 20, 50, and 100 mV s^{-1}.

$$\frac{i_a - i_b}{2} = v \cdot C_{DL} \quad (1)$$

By plotting Δi and scan rate, values of C_{DL} can be determined by the slope. i_a and i_c are the currents at 0.35 V vs. Hg/HgO, v is scan rate.

The TOF of the electrocatalysts were determined by Equ. (2) and (3).

$$n = \frac{m_{mass}}{M} \quad (2)$$

$$TOF = \frac{JA}{4Fn} \quad (3)$$

where n is the number of moles of the active sites (Ni) on the rotating disk electrode, m_{mass} is mass loading of active materials and M is molar mass of active materials, respectively. J is the current density at overpotential of 300 and 350 mV in A cm^{-2}, A is the area of the rotating disk electrode (0.196 cm^{-2}) and F is the Faraday constant (96485 C mol^{-1}). The TOF was calculated assuming a 100% Faradic efficiency.

Acknowledgments

This work was financially supported by the Australian Research Council (ARC) DECRA Grant (DE160100596) and AIIM FOR GOLD Grant (2017, 2018). The authors acknowledge use of facilities within the UOW electron Microscopy Center.

Keywords: $NiMoO_4$, Fe doping, oxygen evolution reaction, water splitting, electrocatalysis

[1] a) Y. P. Zhu, C. Guo, Y. Zheng and S.-Z. Qiao, *Acc. Chem. Res.* **2017**, *50*, 915-923; b) X.-F. Lu, P.-Q. Liao, J.-W. Wang, J.-X. Wu, X.-W. Chen, C.-T. He, J.-P. Zhang, G.-R. Li and X.-M. Chen, *J. Am. Chem. Soc.* **2016**, *138*, 8336-8339.
[2] Y. Lee, J. Suntivich, K. J. May, E. E. Perry and Y. Shao-Horn, *J Phys. Chem. Lett.* **2012**, *3*, 399-404.
[3] a) T. N. Lambert, J. A. Vigil, S. E. White, D. J. Davis, S. J. Limmer, P. D.

Burton, E. N. Coker, T. E. Beechem and M. T. Brumbach, *Chem. Commun.* **2015**, *51*, 9511; b) Y. Zhao, X. Jia, G. Chen, L. Shang, G. I. N. Waterhouse, L. Z. Wu, C. H. Tung, D. O'Hare and T. Zhang, *J. Am. Chem. Soc.* **2016**, *138*, 6517-6524; c) D. K. Bediako, Y. Surendranath and D. G. Nocera, *J. Am. Chem. Soc.* **2013**, *135*, 3662-3674; d) Y. Chen, Q. Zhou, G. Zhao, Z. Yu, X. Wang, S. X. Dou and W. Sun, *Adv. Funct. Mater.* **2018**, *28*, 1705583; e) Q. Zhou, Y. Chen, G. Zhao, Y. Lin, Z. Yu, X. Xu, X. Wang, H. K. Liu, W. Sun and S. X. Dou, *ACS Catalysis* **2018**, *8*, 5382-5390; f) K. Rui, G. Zhao, Y. Chen, Y. Lin, Q. Zhou, J. Chen, J. Zhu, W. Sun, W. Huang and S. X. Dou, *Adv. Funct. Mater.* **2018**, *28*, 1801554.

[4] Z. Lu, W. Xu, W. Zhu, Q. Yang, X. Lei, J. Liu, Y. Li, X. Sun and X. Duan, *Chem. Commun.* **2014**, *50*, 6479-6482.

[5] a) J. Huang, J. Chen, T. Yao, J. He, S. Jiang, Z. Sun, Q. Liu, W. Cheng, F. Hu, Y. Jiang, Z. Pan and S. Wei, *Angew. Chem. Int. Ed.* **2015**, *54*, 8722-8727; b) J.-S. Li, S.-L. Li, Y.-J. Tang, M. Han, Z.-H. Dai, J.-C. Bao and Y.-Q. Lan, *Chem. Commun.* **2015**, *51*, 2710-2713; c) Z. Zhao, H. Wu, H. He, X. Xu and Y. Jin, *Adv. Funct. Mater.* **2014**, *24*, 4698-4705.

[6] a) Y. Liu, H. Cheng, M. Lyu, S. Fan, Q. Liu, W. Zhang, Y. Zhi, C. Wang, C. Xiao, S. Wei, B. Ye and Y. Xie, *J. Am. Chem. Soc.* **2014**, *136*, 15670-15675; b) C. Tang, N. Cheng, Z. Pu, W. Xing and X. Sun, *Angew. Chem.* **2015**, *127*, 9483-9487; c) H. Fan, H. Yu, Y. Zhang, Y. Zheng, Y. Luo, Z. Dai, B. Li, Y. Zong and Q. Yan, *Angew. Chem. Int. Ed.* **2017**, *56*, 12566-12570; d) G. Zhao, P. Li, K. Rui, Y. Chen, S. X. Dou and W. Sun, *Chem. Eur. J. 24*, 11158-11165.

[7] a) A. Azor, M. L. Ruiz-Gonzalez, F. Gonell, C. Laberty-Robert, M. Parras, C. Sanchez, D. Portehault and J. M. González-Calbet, *Chem. Mater.* **2018**; b) W. Yanyong, Z. Yiqiong, L. Zhijuan, X. Chao, F. Shi, L. Dongdong, S. Mingfei and W. Shuangyin, *Angew. Chem. Int. Ed.* **2017**, *56*, 5867-5871; c) K. Xu, P. Chen, X. Li, Y. Tong, H. Ding, X. Wu, W. Chu, Z. Peng, C. Wu and Y. Xie, *J. Am. Chem. Soc.* **2015**, *137*, 4119-4125; d) Z. Sun, T. Liao and L. Kou, *Science China Materials* **2017**, *60*, 1-24; e) J. Mei, Y. Zhang, T. Liao, Z. Sun and S. X. Dou, *National Science Review* **2018**, *5*, 389-416.

[8] R. N. Singh, J. P. Singh and A. Singh, *Int. J. Hydrogen Energy* **2008**, *33*, 4260-4264.

[9] a) D. Friebel, M. W. Louie, M. Bajdich, K. E. Sanwald, Y. Cai, A. M. Wise, M.-J. Cheng, D. Sokaras, T.-C. Weng, R. Alonso-Mori, R. C. Davis, J. R. Bargar, J. K. Nørskov, A. Nilsson and A. T. Bell, *J. Am. Chem. Soc.* **2015**, *137*, 1305-1313; b) L. J. Enman, M. B. Stevens, M. H. Dahan, M. R. Nellist, M. C. Toroker and S. W. Boettcher, *Angew. Chem. Int. Ed.* **2018**, *57*, 12840-12844.

[10] a) B. Wang, S. Li, X. Wu, W. Tian, J. Liu and M. Yu, *J. Mater.Chem. A* **2015**, *3*, 13691-13698; b) X. Wang, H. Xia, J. Gao, B. Shi, Y. Fang and M. Shao, *J. Mater.Chem. A* **2016**, *4*, 18181-18187.

[11] K. Xiao, L. Xia, G. Liu, S. Wang, L.-X. Ding and H. Wang, *J. Mater.Chem. A* **2015**, *3*, 6128-6135.

[12] a) C.-C. Wu and C.-F. Yang, *Nanoscale Res Lett.* **2013**, *8*, 33; b) T. Zhou, Z. Cao, P. Zhang, H. Ma, Z. Gao, H. Wang, Y. Lu, J. He and Y. Zhao, *Sci. Rep.* **2017**, *7*, 46154.

[13] a) Y.-T. Lu, Y.-J. Chien, C.-F. Liu, T.-H. You and C.-C. Hu, *J. Mater.Chem. A* **2017**, *5*, 21016-21026; b) H.-Y. Wang, Y.-Y. Hsu, R. Chen, T.-S. Chan, H.-M. Chen and B. Liu, *Adv. Energy. Mater.* **2015**, *5*, 1500091.

[14] J. Zhang, G. Wang, Z. Liao, P. Zhang, F. Wang, X. Zhuang, E. Zschech and X. Feng, *Nano Energy* **2017**, *40*, 27-33.

[15] a) Z. Wu, Z. Zou, J. Huang and F. Gao, *J. Catal.* **2018**, *358*, 243-252; b) J. Y. C. Chen, L. Dang, H. Liang, W. Bi, J. B. Gerken, S. Jin, E. E. Alp and S. S. Stahl, *J. Am. Chem. Soc.* **2015**, *137*, 15090-15093.

[16] D. K. Bediako, Y. Surendranath and D. G. Nocera, *J. Am. Chem. Soc.* **2013**, *135*, 3662-3674.

[17] a) F. Song and X. Hu, *Nature Communications* **2014**, *5*, 4477; b) C. C. L. McCrory, S. Jung, J. C. Peters and T. F. Jaramillo, *J. Am. Chem. Soc.* **2013**, *135*, 16977-16987; c) J. A. Carrasco, J. Romero, M. Varela, F. Hauke, G. Abellán, A. Hirsch and E. Coronado, *Inorganic Chemistry Frontiers* **2016**, *3*, 478-487; d) G. Abellán, J. A. Carrasco, E. Coronado, J. Romero and M. Varela, *Journal of Materials Chemistry C* **2014**, *2*, 3723-3731.

[18] a) M. Tahir, L. Pan, R. Zhang, Y.-C. Wang, G. Shen, I. Aslam, M. A. Qadeer, N. Mahmood, W. Xu, L. Wang, X. Zhang and J.-J. Zou, *ACS Energy Letters* **2017**, *2*, 2177-2182; b) X. Zheng, B. Zhang, P. De Luna, Y. Liang, R. Comin, O. Voznyy, L. Han, F. P. García de Arquer, M. Liu, C. T. Dinh, T. Regier, J. J. Dynes, S. He, H. L. Xin, H. Peng, D. Prendergast, X. Du and E. H. Sargent, *Nature Chemistry* **2017**, *10*, 149.

[19] H. M. Sun, Y. X. Ye, Z. F. Tian, S. L. Wu, J. Liu and C. H. Liang, *RSC Advances* **2017**, *7*, 49010-49014.

[20] a) M. Ciureanu, S. D. Mikhailenko and S. Kaliaguine, *Catal. Today* **2003**, *82*, 195-206; b) L. Trotochaud, S. L. Young, J. K. Ranney and S. W. Boettcher, *J. Am. Chem. Soc.* **2014**, *136*, 6744-6753.

[21] a) V. Vij, S. Sultan, A. M. Harzandi, A. Meena, J. N. Tiwari, W.-G. Lee, T. Yoon and K. S. Kim, *ACS Catalysis* **2017**, *7*, 7196-7225; b) K. Fominykh, J. M. Feckl, J. Sicklinger, M. Döblinger, S. Böcklein, J. Ziegler, L. Peter, J. Rathousky, E. W. Scheidt, T. Bein and D. Fattakhova Rohlfing, *Adv. Funct. Mater.* **2014**, *24*, 3123-3129.

[22] a) Z. Dai, H. Geng, J. Wang, Y. Luo, B. Li, Y. Zong, J. Yang, Y. Guo, Y. Zheng, X. Wang and Q. Yan, *ACS Nano* **2017**, *11*, 11031-11040; b) M. Justus, S. Ilya, M. Hemma, V. Edgar, d. l. M. Maria, A. Jordi, M. Martin, R. C. Beatriz and S. Wolfgang, *Adv. Energy. Mater.* **2017**, *7*, 1700381; c) L.-A. Stern, L. Feng, F. Song and X. Hu, *Energy Environ. Sci.* **2015**, *8*, 2347-2351.

[23] a) M. Görlin, P. Chernev, J. Ferreira de Araújo, T. Reier, S. Dresp, B. Paul, R. Krähnert, H. Dau and P. Strasser, *J. Am. Chem. Soc.* **2016**, *138*, 5603-5614; b) J. Landon, E. Demeter, N. İnoğlu, C. Keturakis, I. E. Wachs, R. Vasić, A. I. Frenkel and J. R. Kitchin, *ACS Catalysis* **2012**, *2*, 1793-1801; c) K. Fominykh, P. Chernev, I. Zaharieva, J. Sicklinger, G. Stefanic, M. Döblinger, A. Müller, A. Pokharel, S. Böcklein, C. Scheu, T. Bein and D. Fattakhova-Rohlfing, *ACS Nano* **2015**, *9*, 5180-5188.

Entry for the Table of Contents

Layout 1:

FULL PAPER

Fe-doped $NiMoO_4$ was synthesized toward enhanced alkaline OER. The excellent catalytic activity can be attributed to the high valence Ni^{3+} species induced by Fe doping, benefiting the formation of Ni^{3+}-OOH. The results provide new alternatives to precious metal-free catalysts for alkaline OER.

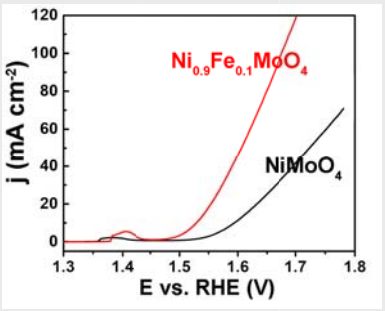

Jiayi Chen, Guoqiang Zhao, Yaping Chen, Kun Rui, Hui Mao, Shi Xue Dou, and Wenping Sun**

Page No. – Page No.

Iron-doped nickel molybdate with enhanced oxygen evolution kinetics